Determination of long range antiferromagnetic order by powder neutron diffraction

Practical course on powder diffraction at the neutron spallation source SINQ of the Paul Scherrer Institute

Summary

Antiferromagnetic (AFM) ordering of Mn spins in manganese sulfide MnS or manganese oxide MnO will be determined by powder neutron diffraction. These compounds crystallize in a rock salt face centered cubic crystal structure. Manganese sulfide MnS shows a transition to the AFM state with the propagation vector $\vec{k}$=(½, ½, ½) at the Néel temperature of about 150 K. The Mn-spins forming planes perpendicular to the body diagonal are ferromagnetically aligned, whereas the spins in the neighboring planes are antiparallel.

During the practicum we will try to reproduce one of the neutron diffraction experiments performed during 1946-1951 for which C.G. Shull was honored with the Nobel Prize in 1994. We will perform neutron diffraction experiment with MnS using powder diffractometer HRPT at the neutron source SINQ of the Paul Scherrer Institute. From the analysis of the nuclear and magnetic Bragg peak intensities and positions we will verify the crystal and magnetic structures of manganese sulfide and determine the size of the magnetic moment on manganese.

Note: The practicum is performed during only one day at PSI. To perform the experiment effectively and analyze the experimental data it is necessary to have basic theoretical background on mathematical description of crystal structure and diffraction (reciprocal space, Brillouin zone, structure factor, etc.).

Some relevant lectures

V. Pomjakushin , *"Determination of the magnetic structure from powder neutron diffraction"*
Lecture given at the "Workshop on X-rays, Synchrotron Radiation and Neutron Diffraction Techniques", June 18-22, 2008, Paul Scherrer Institut, Villigen, Switzerland"

Download: as it is (pdf 11 Mb), compacted slides (pdf 9 Mb) or mov

V. Pomjakushin , *"Advanced magnetic structures: classification and determination by neutron diffraction"* (Exercize)
Lecture given on 24.03.2010 at the ETHZ lecture course "Neutron Scattering in Condensed Matter Physics" of Prof. A.Zheludev

Download: pdf 18 Mb

V. Pomjakushin , *"High Resolution Powder Diffractometer for Thermal Neutrons"*
Talk given at the AIC Information Day on "Large Facilities for Crystallography Studies: Synchrotron and Neutron sources", October 19th, 2009 , Paul Scherrer Institut, Villigen, Switzerland

Download: pdf 31 Mb

Table of content

Magnetic ordering phenomena

Magnetic order in MnS

MAGNETIC ORDERING PHENOMENA

1 Introduction

A magnetic structure is a periodic arrangement of magnetic moments in a crystalline material. This implies that magnetic materials are composed of periodic arrangements of vectorial spin densities superimposed on periodic arrangements of atoms with scalar charge- or nuclear-densities. The order of the latter densities (crystal structure) is determined by x-ray or neutron diffraction. The order of the former can also be studied by these techniques. But despite the impressive progress of synchrotron radiation sources and techniques, x-ray scattering is still rather a complementary new tool in magnetism, and neutron scattering is the experimental method of choice for studying magnetic structures in condensed matter on an atomic scale.

2 Magnetic interactions

The magnetic order in crystalline material is governed by the competition between the exchange interactions and the magnetic anisotropy.

The magnetic interaction, which arises from the direct Coulomb interaction among electrons from two ions (Fig. 1), is known as *direct exchange*. Even though this is referred to as a magnetic interaction one should not be lulled by this nomenclature into forgetting that underlying the exchange interaction are nothing but electrostatic interaction energies and the Pauli exclusion principle. It often happens that two magnetic ions are separated by a nonmagnetic ion (i.e. one with all electronic shells closed). It is then possible for the magnetic ions to have a magnetic interaction mediated by the electrons in their common nonmagnetic neighbors, which is more important than their direct exchange interaction. This type of magnetic interaction is called *superexchange*.
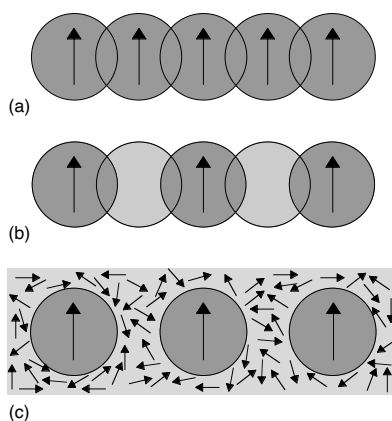
Figure 1: Schematic illustrations of (a) direct exchange, in which the magnetic ions interact because their charge distribution overlap; (b) superexchange, in which magnetic ions with non-overlapping charge distributions interact because both have overlap with the same nonmagnetic ion; and (c) indirect exchange, in which in the absence of overlap a magnetic interaction is mediated by interactions with the conduction electrons.

The magnetic interactions that are present in insulators, direct and superexchange, are short-range interactions. Yet another source of magnetic interaction can occur in metals. In addition to their direct exchange coupling, the electrons of the partially filled shells of the magnetic ions are coupled through their interactions with conduction electrons. This

mechanism (in a sense the metallic analogue of superexchange in insulators) is known as *indirect exchange*. It can be stronger than the direct exchange coupling, especially in rare-earth metals since the f-shells generally overlap very little. Such an interaction by polarization of conduction electrons, the RKKY interaction [1], is long-range and oscillatory. One should also mention that there are also important exchange interactions in metals among the conduction electrons themselves, often referred to as *itinerant exchange*.

The exchange interaction depends on the mutual orientation of the magnetic moments and on the distance between magnetic atoms. At moderate temperatures thermal motion of the magnetic moments is usually stronger than the exchange interaction energies and prevents magnetic order on a macroscopic time scale. The magnetic moments are then randomly oriented, i.e. disordered. Such a magnetic state is called paramagnetism. Below a critical temperature for magnetic ordering (Curie temperature T_C or Néel temperature T_N) the magnetic interaction may prevail and long-range magnetic ordering in Weiss domains of magnetic materials occurs. A positive exchange constant J_{ij} between two moments on sites i and j favors parallel alignment of the spins (ferromagnetism), whereas negative J_{ij} would yield the lowest energy for antiparallel orientation of the spins, i.e. for antiferromagnetic coupling.

These exchange interactions are in competition with the magnetic anisotropy due to crystalline electric field effects [2]. The resulting magnetic structures can be quite complex, even for elements [3], and depend strongly on external parameters such as temperature, magnetic field and pressure. In the following some examples of magnetic structures observed in rare-earth compounds are discussed and the role of neutron scattering, with emphasis on powder neutron diffraction, in the analysis of magnetic ordering is shown.

3 Magnetic order and neutron diffraction

A neutron diffraction study of a magnetic structure does not start from scratch. One usually bases the study on available information from bulk magnetic measurements, which means that one at least knows the ordering temperature and the temperature dependence of the average susceptibility. It is also a good approach to perform a symmetry analysis that predicts possible incipient magnetic structures consistent with the crystalline space group. Three-dimensional long-range magnetic ordering leads to coherent scattering in neutron diffraction experiments and to Bragg peaks in the neutron diffraction pattern. The magnetic unit cell determines the positions of these peaks (as the chemical unit cell determines the positions of the nuclear Bragg peaks). Therefore an analysis of the magnetic Bragg peak positions is always the first step in the analysis of a magnetic structure in order to derive the magnetic unit cell. The magnetic moment arrangement in the cells, i.e. the magnetic structure factor, determines the peak intensity, in analogy to the nuclear structure factor for nuclear scattering.

The magnetic neutron scattering is caused by the interaction of the magnetic moment $\hat{\mu}_n$ of the neutron and the atomic magnetic moments

$$\hat{\mu} = -\mu_B(\hat{L} + 2\hat{S}) \qquad (1)$$

due to unpaired electrons. $\hat{L}$ denotes the orbital angular momentum operator $\hat{r} \times \hat{p}$ and $\hat{S}$ the spin angular momentum operator.

In the case of unpaired d-electrons such as $3d^5$ of an Fe^{3+} ion in a solid, the orbital momentum is generally quenched by the crystalline electric field, and thus the maximum magnetic moment component $<\hat{\mu}_z> = gS = 5 \mu_B$ ($g \approx 2$, S = 5/2). On the other hand for unpaired f-electrons such as $4f^{10}$ of the rare-earth ion Ho^{3+} one has a $^5I_8$ ground state of the free ion, i.e. S = 2, L = 6 and J = L + S. These values yield a maximum $<\hat{\mu}_z> = gJ = 10 \mu_B$ (g = 5/4, J = 8). Generally the ordered magnetic f-electron moments of rare-earth ions in crystals are reduced below the values of free ions due to the crystalline electric field splitting of the ground state, which may be measured by means of inelastic neutron scattering [2]. In addition, hybridization

effects of f-electrons and conduction electrons in strongly correlated electron systems, like the Kondo compound $CePd_2Ga_3$ [4], may further reduce the ordered moment and ordering temperature, or even suppress magnetic ordering at all.

3.1 Paramagnetism

As mentioned above, in the paramagnetic state the magnetic moments are randomly oriented, i.e. disordered. The differential magnetic cross section for a Bravais lattice paramagnet consisting of a single type of magnetic J state ions can be derived from the general cross section for magnetic neutron scattering [5] and reads as

$$\left(\frac{d\sigma}{d\Omega}\right)^{para}_{mag} = \frac{2}{3} N(pge^{-W})^2 F^2(Q)J(J+1) \tag{2}$$

with $p = \gamma e^2/(2m_e c^2)$. The paramagnetic scattering is purely incoherent with an intensity contribution to the background that is proportional to $J(J+1)$. Moreover the paramagnetic intensity diminishes with increasing scattering vector $\mathbf{Q}$ proportional to the square of the neutron magnetic form factor $F(Q)$ (Fig. 2) which is the Fourier transform of the magnetic potential.
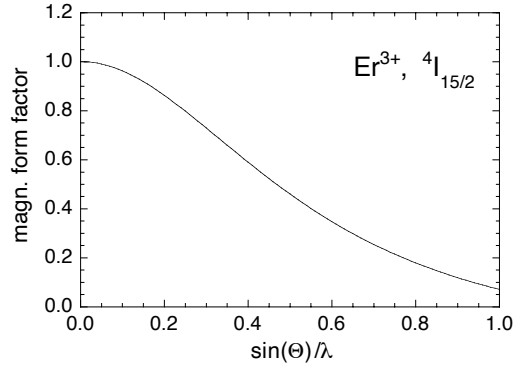
Figure 2: Magnetic form factor for the trivalent rare-earth ion Er^{3+} (dipole approximation) with ground state $^4I_{15/2}$.

In the dipole approximation the magnetic form factor $F(Q)$ reads as

$$F(Q) = <j_0(Q)> + <j_2(Q)> \frac{J(J+1) + L(L+1) - S(S+1)}{3J(J+1) - L(L+1) + S(S+1)} \tag{3}$$

with radial integrals $<j_v>$ calculated in relativistic Dirac-Fock formalism and tabulated in [6].

3.2 Ferromagnetism

In the absence of an external magnetic field a ferromagnetic crystal is composed of small regions, or domains, in each of which the electron spins tend to align in the same direction. The cross section for a sample with many domains is

$$\left(\frac{d\sigma}{d\Omega}\right)^{ferro}_{mag} = N \frac{(2\pi)^3}{V_0} \langle S \rangle^2 \sum_\tau \left[1 - \left(\tilde{\boldsymbol{\tau}} \cdot \tilde{\boldsymbol{\eta}}\right)^2\right] |F_M|^2 \delta(\mathbf{Q} - \boldsymbol{\tau}) \tag{4a}$$

$$|F_M|^2 = \left[pgF(Q)e^{-W}\right]^2 \tag{4b}$$

where $\tilde{\eta}$ is a unit vector in the direction of the magnetic moment and $\tilde{\tau}$ is a unit vector in the direction of the reciprocal lattice vector τ.

Using α as angle between the spin direction and $\tilde{\tau}$, $1-(\tilde{\tau}\cdot\tilde{\eta})^2$ is equal to $\sin^2\alpha$, i.e. the spin component perpendicular to τ determines the magnetic intensity. We see from the δ-functions in Eq. (4a) that for a ferromagnetic crystal the magnetic Bragg peaks occur at the same points in reciprocal space as the nuclear Bragg peaks. However, there are several important differences between magnetic and nuclear Bragg scattering. Firstly, the magnetic scattering, being proportional to $\langle S\rangle^2$, is very temperature dependent, and falls to zero at the Curie temperature T_C. The nuclear scattering varies little with temperature; the only term in the cross section that is temperature dependent is the Debye-Waller factor. Secondly, for magnetic scattering, the magnetic form factor $F(Q)$ falls rapidly with increasing Q (Fig. 2). This is because the form factor is the Fourier transform of the magnetic potential, and the latter has a long range. The nuclear potential on the other hand has a very short range, and its Fourier transform is virtually independent of Q.

An example for a ferromagnetic compound is the rare-earth trichloride $TbCl_3$ which orders in the orthorhombic space group Cmcm. This compound has been investigated by neutron diffraction measurements on polycrystalline samples [7]. Below $T_C = 3.7$ K long-range ferromagnetic order was found (Fig. 3), and the refinement of the data yielded a large saturation moment of 8.4 μ_B per Tb^{3+} ion and an alignment of the magnetic moments perpendicular to the c axis.
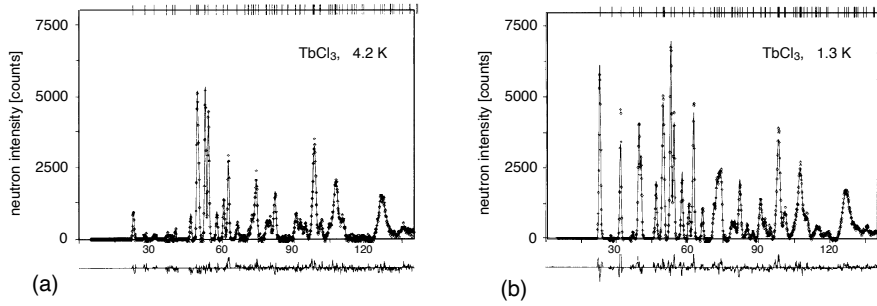
Figure 3: (a) Observed (points, a linear background has been subtracted) and calculated (line) neutron diffraction intensities of paramagnetic $TbCl_3$ at 4.2 K. (b) Observed (points) and calculated (line) neutron diffraction patterns of ferromagnetic $TbCl_3$ at 1.3 K.

3.3 Collinear antiferromagnetism

For a commensurate collinear antiferromagnet consisting of two sublattices A and B with antiparallel spin alignment, one obtains

$$\left(\frac{d\sigma}{d\Omega}\right)_{mag}^{antiferro} = N_M \frac{(2\pi)^3}{V_{0M}} \langle S\rangle^2 \sum_{\tau}\left[1-(\tilde{\tau}_M\cdot\tilde{\eta})^2\right]|F_M|^2\delta(\mathbf{Q}-\tau_M) \qquad (5a)$$

$$|F_M|^2 = [pgF(Q)e^{-W}]^2\left|\sum_{v}\sigma_v e^{i\mathbf{Q}\cdot\tau_v}\right|^2 \qquad (5b)$$

where $\sigma_v = +1$ for an ion in sublattice A and $\sigma_v = -1$ for an ion in sublattice B.

We can see from the δ-functions in Eq. (5a) that now the magnetic Bragg peaks appear at positions corresponding to the magnetic unit cell in reciprocal space. Because of magnetic unit cells that are larger than the chemical cell and due to new extinction rules, generally new antiferromagnetic Bragg reflections appear in the ordered state.

7
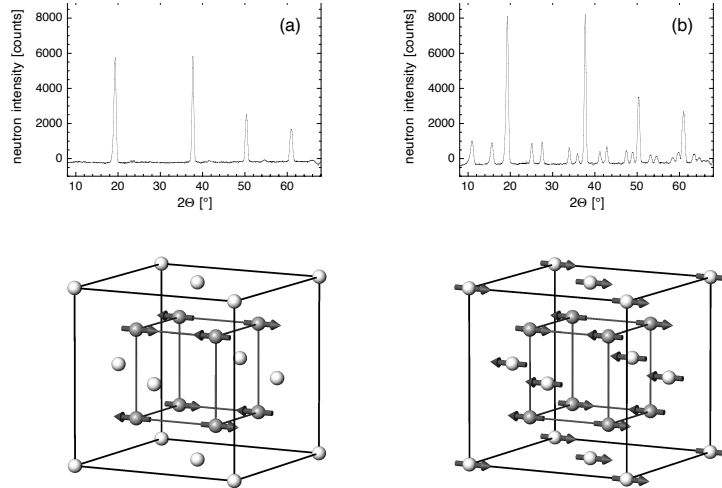
Figure 4: (a) Neutron diffraction pattern (magnetic scattering only) and corresponding magnetic structure in $Nd_3Pd_{20}Ge_6$ below $T_{N1} = 1.75$ K. While the Nd moments on one site are antiferromagnetically ordered, the moments on the other site remain disordered. (b) Magnetic neutron diffraction pattern and corresponding magnetic structure below $T_{N2} = 0.58$ K; also the second Nd sublattice is magnetically ordered.

Antiferromagnetism has been observed in many rare-earth compounds, recent examples are the new cubic compounds of the general composition $R_3Pd_{20}X_6$ (R = rare earth; X = Pd, Si). These systems crystallize in the cubic space group $Fm\bar{3}m$ in which the rare-earth ions possess two crystallographically different sites, 4a and 8c, respectively. Looking only at the magnetic ions, the crystallographic structure may be viewed as built up by two interpenetrating sublattices, each one formed by the rare-earth ions on each sites. Bulk magnetic measurements revealed two magnetic phase transitions (T_{N1} and T_{N2}) and neutron diffraction experiments, e.g. for $Nd_3Pd_{20}Ge_6$ [8], found that the two sublattices undergo independent magnetic phase transitions to long-range antiferromagnetic order at T_{N1} and T_{N2}. In the temperature range $T_{N1} > T > T_{N2}$, a coexistence was found of antiferromagnetic ordering of ions on site 8c with disordered moments on the site 4a. At T_{N2} the sublattice formed by ions on 4a sites also undergoes a phase transition to antiferromagnetic order.

3.4   Incommensurate magnetic structures

In metallic rare-earth compounds the principal interaction which couples the magnetic moments is indirect RKKY-type exchange. The long range and oscillatory character of this coupling may compete with other interactions, for example the crystal field anisotropy or even weaker interactions like magnetoelastic coupling or two-ion quadrupolar interactions. The interplay between these competing interactions may lead to incommensurate or amplitude-modulated magnetic structures and complex magnetic phase diagrams. Incommensurate magnetic structures have periodicities that do not match the periodicity of the crystal lattice.
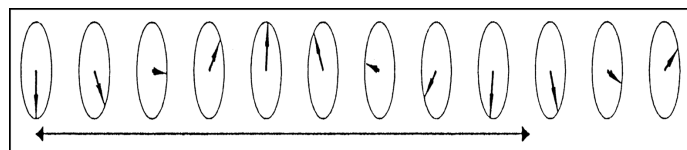
Figure 5: Schematic view of a simple spiral magnetic structure (helix). The long horizontal arrow shows the repeat distance.

It can be shown that the elastic magnetic neutron scattering cross section for e.g. an incommensurate spiral structure (Fig. 5) is

$$\left(\frac{d\sigma}{d\Omega}\right)^{spiral}_{mag} = \frac{1}{4} N \frac{(2\pi)^3}{V_0} \left[pgF(Q)e^{-W}\right]^2 \langle S \rangle^2 \sum_\tau \left[\delta(\mathbf{Q}+\mathbf{K}-\tau) + \delta(\mathbf{Q}-\mathbf{K}-\tau)\right] \quad (6)$$

Eq. (6) shows that magnetic Bragg scattering occurs when $\mathbf{Q} = \tau \pm \mathbf{K}$. Thus each nuclear Bragg peak $\mathbf{Q} = \tau$ is accompanied by a pair of magnetic satellites (Fig. 6). The periodicity of an incommensurate magnetic structure is usually described by the magnetic propagation vector $\mathbf{k} = (k_1, k_2, k_3)$, where k_i are the components of $\mathbf{K}$ in reciprocal lattice units.
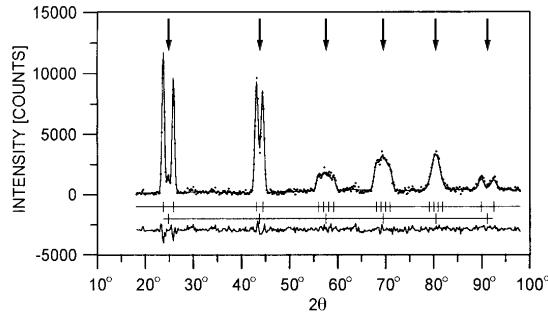
Figure 6: ErGa$_3$: Observed (points) and calculated (line) magnetic difference neutron diffraction pattern showing the magnetic peaks only (satellites). The arrows indicate the nuclear peak positions.

The magnetic ordering of Er moments in ErGa$_3$ has recently been investigated by powder and single crystal neutron diffraction [9]. The diffraction pattern is characterized by the presence of satellite peaks, at positions that do not coincide with reciprocal lattice points either of the chemical cell or any simple multiple of it. As no higher order satellites were detected, the models considered were restricted to sinusoidal modulated types. The incommensurate magnetic structure of ErGa$_3$ has been satisfactorily described by a single propagation vector $\mathbf{k} = [1/2+\delta, 1/2, 0]$, $\delta = 0.042$. It can be viewed as an antiferromagnetic structure corresponding to $\mathbf{k} = [1/2, 1/2, 0]$, i.e. doubling of the cell in a and b directions, superimposed by a sinusoidal incommensurate modulation along a.

Another example of incommensurate ordering in rare-earth compounds is PrPdAl [10]. In this compound the rare-earth ions are arranged on a triangular lattice which hinders the formation of the antiferromagnetic spin arrangement favored by the exchange interactions. The magnetic structure of such a geometrical frustration system is driven by the competition of geometrical restrictions and exchange couplings. In PrPdAl this results in a remarkable reduction of the ordered moments in the ab-plane as well as an incommensurate modulation along c.

4   Concluding remarks

Neutron diffraction is a powerful method for measuring magnetic ordering and analyzing magnetic structures. It has been one of the most important tools in the wide field of rare-earth magnetism in the past - and it still is, as the very recent examples in this chapter show. Even though examples of neutron powder experiments were given here it must be noted that for most complicated magnetic structures single crystal experiments are required in order to unambiguously determine the correct magnetic order.

Neutron scattering is the reference technique for probing long-range order formed on a lattice of atoms or magnetic moments. Under certain conditions it can also be invaluable for studying more exotic types of ordered structures involving electron charge distributions. One of them is quadrupolar ordering. Besides their magnetic dipole moments, lanthanide elements with incomplete 4f electron shells are known to also possess higher-order moments (quadrupole, octupole, etc.). In a classical picture, this reflects the non-sphericity of the electron charge distribution. In the case of solids, pair interactions between 4f quadrupoles located at neighboring sites can occur either directly through their electrostatic potentials (usually weak), or indirectly through various channels such as lattice strains (cooperative Jahn-Teller effect), conduction electrons in metals (RKKY-type coupling), higher-order exchange terms, etc. For most real systems, conventional magnetic interactions dominate, and the 4f dipole-moment lattice orders in a long-range magnetic structure at low temperature. Accordingly, the quadrupole moments will have non-zero values in the magnetic state, but this is only the result of dipole ordering. More rarely, quadrupole interactions can prevail and produce a phase transition on their own, whose primary order parameter is a component, or a combination of components, of the quadrupole tensor. It has been demonstrated in several systems such as TmTe [11] that neutron diffraction, combined with a large external magnetic field, can provide a powerful (but indirect) tool for studying quadrupolar order in solids.

References

1. M.A. Rudermann and C. Kittel, *Phys. Rev.* **96**, 99 (1954); T. Kasuya, *Prog. Theo. Phys. Japan* **16**, 45 (1956); K. Yosida, *Phys. Rev.* **106**, 893 (1957).
2. A. Mirmelstein, this volume.
3. J. Jensen and A.R. Mackintosh, *Rare Earth Magnetism* (Clarendon Press, Oxford, 1991).
4. E. Bauer, G. Schaudy, G. Hilscher, L. Keller, P. Fischer and A. Dönni, *Z. Phys. B* **94**, 359 (1994).
5. G.L. Squires, *Introduction to the Theory of Thermal Neutron Scattering* (Dover Publications, New York, 1996).
6. P.J. Brown, *Int. Tables for Crystallography C*, ed. A.J.C. Wilson (Kluwer Academic Publ., Dordrecht, 1992) p. 391.
7. A. Murasik, P. Fischer and A. Furrer, *J. Less-Comm. Metals* **111**, 177 (1984).
8. A. Dönni, F. Fauth, P. Fischer, T. Herrmannsdörfer, L. Keller and T. Komatsubara, *J. Alloys Comp.* **306**, 40 (2000).
9. A. Murasik, A. Czopnik, L. Keller and P. Fischer, *J. Magn. Magn. Mater.* **213**, 101 (2000); A. Murasik, A. Czopnik, L. Keller and P. Fischer, *phys. stat. sol. (a)* **173**, R1 (1999).
10. L. Keller, A. Dönni, H. Kitazawa, J. Tang, F. Fauth and M. Zolliker, *Physica B* **241-243** (1998) 660; L. Keller, A. Dönni and H. Kitazawa, *Physica B* **276-278**, 672 (2000).
11. P. Link, A. Gukasov, J.-M. Mignot, T. Matsumara and T. Suzuki, *Phys. Rev. Lett.* **80**, 4779 (1998).

MAGNETIC ORDER IN MnS

5. Practical course at SINQ

5.1 Manganese sulfide MnS

- rock salt crystal structure
- ionic crystal: Mn^{2+}, S^{2-}
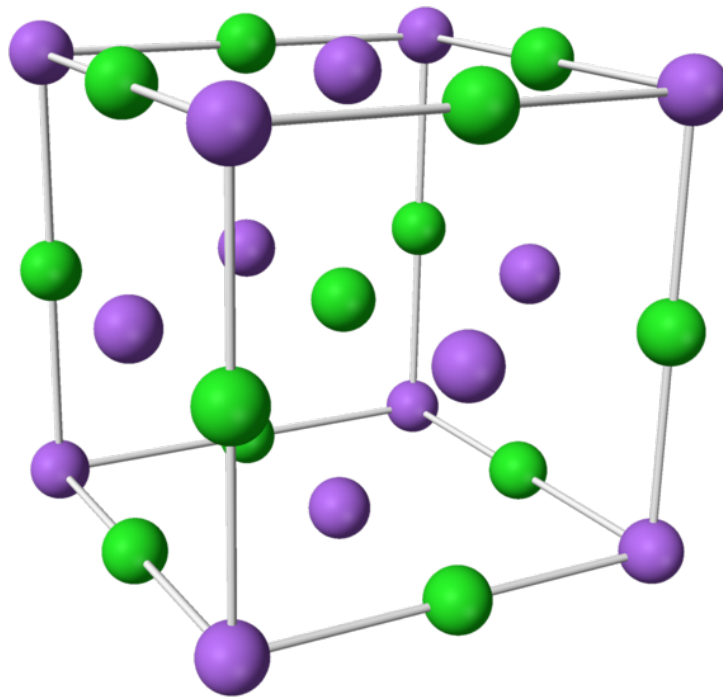
- lattice constant a = 5.199 Å at T = 4.2 K
- space group $Fm\bar{3}m$
- electronic configuration of Mn^{2+}: $3d^5$
- Néel temperature T_N = 161 K
- long-range antiferromagnetic order: antiferromagnetic stacking along (111) of ferromagnetic planes
- therefore doubling of the magnetic unit cell with respect to the crystallographic unit cell

5.2 Neutron diffraction of MnS at room temperature

$$\lambda = 2d_{hkl} \sin \theta_{hkl} \qquad\qquad\qquad \text{Bragg law}$$

λ: neutron wavelength, d_{hkl}: d-spacing of scattering plane hkl
θ_{hkl}: (half) scattering angle of reflection hkl in diffraction pattern

$$d_{hkl} = \frac{a}{\sqrt{h^2 + k^2 + l^2}}$$

a: cubic lattice constant, h, k, l indices of scattering plane

$$\vec{\tau}_{hkl} = \frac{2\pi}{a}(h, k, l)$$

corresponding vector in reciprocal space

Tasks:

- measure a diffraction pattern of MnS in the paramagnetic state, e.g. at T = 250 K

-determine peak positions Θ, d-spacings and indices (h, k, l) for all observed peaks

Coherent elastic cross section for nuclear neutron diffraction:

$$\frac{d\sigma}{d\Omega} \sim \sum_{\vec{\tau}_{hkl}} \left|F_{\vec{\tau}_{hkl}}\right|^2 \delta(\vec{Q} - \vec{\tau}_{hkl})$$

$\vec{Q}$: scattering vector, $\vec{\tau}_{hkl}$: reciprocal lattice vector defining scattering planes
$\delta(\vec{Q} - \vec{\tau}_{hkl})$ → **peak position given by crystal lattice (unit cell)**
$F_{\vec{\tau}_{hkl}}$: structure factor of unit cell

$$F_{\vec{\tau}_{hkl}} = \sum_{\vec{d}_i} b_{\vec{d}_i} e^{i\vec{\tau}_{hkl} \cdot \vec{d}_i}$$

$\vec{d}_i$: atomic coordinate of i-th atom in real space, sum runs over all atoms in unit cell
$b_{\vec{d}_i}$: scattering length of atom at position $\vec{d}_i$

Intensity $\sim \left|F_{\vec{\tau}_{hkl}}\right|^2$ → **peak intensity is mainly given by arrangement of atoms in unit cell**

For cylindrical geometry of the powder sample container the integrated intensity of the scattered neutrons of the Bragg peak at $|\vec{Q}|$ is given by

$$I(Q) = C \cdot A(\theta) \cdot L(\theta) \cdot \frac{d\sigma}{d\Omega} = C \cdot A(\theta) \cdot L(\theta) \cdot F^2(Q) \cdot mult$$

C: scale factor, $A(\theta)$: absorption factor, $L(\theta)$: Lorentz factor, $mult$: multiplicity

$$L(\theta) = \frac{1}{\sin\theta \sin 2\theta}$$

The Lorentz factor $L(\theta)$ is a geometrical correction depending on the scattering geometry.

For MnS: $b_{Mn} = $ -3.73 fm, $b_S = $ 2.85 fm

$\vec{d}$-vectors: Mn: $\vec{d}_1 = $ a(0, 0, 0) $\vec{d}_2 = $ a(0, ½, ½)

$\vec{d}_3 = $ a(½, 0, ½) $\vec{d}_4 = $ a(½, ½, 0)

S: $\vec{d}_5 = $ a(½, ½, ½) $\vec{d}_6 = $ a(½, 0, 0)

$\vec{d}_7 = $ a(0, ½, 0) $\vec{d}_8 = $ a(0, 0, ½)

Tasks:

- calculate $\left|F_{\vec{\tau}_{hkl}}\right|^2$ for (h, k, l) = (1,1,1), calculate the multiplicity

- calculate $\left|F_{\vec{\tau}_{hkl}}\right|^2$ for (h, k, l) = (2,0,0), calculate the multiplicity

- compare ratio of $I(\vec{\tau}_{111}) / I(\vec{\tau}_{200})$ with the measured intensity ratio

5.3 Neutron diffraction of MnS in the magnetically ordered state

Tasks:

- measure a diffraction pattern of MnS in the magnetically ordered state, e.g. at T = 10 K

- compare this date with the paramagnetic pattern at room temperature

- index the magnetic peaks, i.e. find (h, k, l) for each magnetic peak

- based on the indices, what is the magnetic unit cell compared to the crystallographic one

- which magnetic structure, i.e. which arrangement of the magnetic moments, is compatible with the magnetic unit cell

- determine the critical temperature for the onset of magnetic order in MnS by measuring the temperature dependence of the magnetic order

Coherent elastic cross section for collinear antiferromagnetic order

$$\frac{d\sigma}{d\Omega} \sim \sum_{\vec{\tau}_{M,hkl}} \left|F_{M,hkl}\right|^2 \delta(\vec{Q} - \vec{\tau}_{M,hkl})$$

$F_{M,hkl}$: antiferromagnetic structure factor

The intensity of the magnetic Bragg peak at $\left|\vec{Q}_M\right|$ is

$$I(Q_M) = C \cdot A(\theta) \cdot L(\theta) \cdot \left|\vec{F}_{M\perp}\right|^2 \cdot mult$$

where

$$\vec{F}_{M\perp} = \frac{1}{2} r_0 \sum_j e^{i\vec{Q}_M \cdot \vec{d}_j} \vec{\mu}_{j\perp} \quad \text{and} \quad \vec{\mu}_\perp = \left(\vec{\mu} - \frac{\vec{Q}_M(\vec{\mu} \cdot \vec{Q}_M)}{Q_M^2}\right)$$

where $\vec{\mu}_j$ is the magnetic moment in units μ_B of atom at position $\vec{r}_j$ and r_0 = -0.54·10^{-12} cm, $\vec{Q}_M \equiv \vec{\tau}_{M,hkl}$